This is a peer-reviewed, author's accepted manuscript of the following research article:
Nguyen, T., Yesilkaya, A., Chen, C., & Haas, H. (2022). A novel mobile multi-user LiFi system.
In ICC 2022 - IEEE International Conference on Communications (pp. 589-594). [9838651] IEEE.
https://doi.org/10.1109/ICC45855.2022.9838651

A novel mobile multi-user LiFi system

Trang Nguyen, Anil Yesilkaya, Cheng Chen, and Harald Haas
The University of Strathclyde, Department of Electronic & Electrical Engineering,
LiFi Research and Development Centre, Technology & Innovation Centre, 99 George Street, G1 1RD
Email: {trang.nguyen, a.yesilkaya, c.chen, harald.haas}@strath.ac.uk

***Abstract*—In this paper, a vehicular light-fidelity (LiFi) system, which supports mobility for seamless broadband data transmission is proposed for multipoint-to-point (M2P) communication. To this end, a novel digital mirror device (DMD) based receiver (RX) is investigated that consists of two functionalities, to sense the transmitters and sense mobility. Relying on the proposed hybrid waveform, the proposed RX has the ability to detect and distinguish multiple transmitter (TX) sources under free movement conditions within three-dimensional space. Computer simulation results for the 'TX sensing platform' show that a high TX detection and identification performance is achieved at an extremely low channel signal-to-noise-ratio (SNR) of -11 dB and a bit error ratio (BER) of 10^{-4}. Furthermore. the simulation results for the 'mobility sensing platform' was able to trace the positions of light sources simultaneously with the error rate of below 2% relative to the diameter of light spots on the DMD for all considered mobility scenarios.**

***Index Terms*—mobile LiFi, multipoint-to-point (M2P), receiver architecture, hybrid waveform, light sources identification, mobility sensing, digital mirror device (DMD).**

I. Introduction

The advancements in solid-state lighting technologies paved the way for light communication (LC) to be a promising broadband wireless telecommunication solution to fulfil the ever-growing demand of wireless traffic [1]. The radio frequency (RF) non-interfering nature of the light spectrum brings significant advantages, such as a spatial dense and simultaneous spectral reuse to cope with the surge in wirelss data capacity. There are a wide range of LC technologies [2], in which light-fidelity (LiFi) targets short/mid-range solutions where off-the-shelf light emitting diodes (LEDs) and photodiodes (PDs) could be utilized. More specifically, LiFi aims to provide a bi-directional seamless networking solution, by using either the visible light (VL) or infra-red (IR) or both bands, to complement its RF counterparts. As the commercial vehicles are already started to be equipped with radar, sonar, multiple cameras, global positioning system (GPS) and both IR and VL light sources [3], LC is becoming one of the key solutions for efficient vehicular communications. The future of smart vehicles are envisaged with the concepts of vehicle-to-vehicle (V2V) and vehicle-to-infrastructure (V2X). Despite of the prospect of LC, there remain various unmitigated technical challenges in V2V/V2X scenarios as follows:

Harald Haas acknowledges the financial support from the Wolfson Foundation and the Royal Society. All authors acknowledge the financial support from the Engineering and Physical Sciences Research Council (EPSRC) under Established Career Fellowship grant EP/R007101/1.

Initial challenges come with the detection of light sources and the identification of them in a noisy channel condition:

- The first challenge is to detect transmitters (TXs) among other noisy sources. Assume that within the receiver, the beams are spatially separated by the lens and the receiver (RX) can independently process the individual beams; the requirement is to detect TXs among other noisy light sources. However, there are over a hundred light sources being seen by a car but only some of them may be transmitting data and are, therefore, of interest. These are TXs while the others are noisy sources. Noisy sources include the constant-intensity sources such as ambient lights or other non-data flickering sources as well as the data-transmitting sources but from other networks.
- The second challenge is to identify TXs when the channel signal-to-noise-ratio (SNR) is extremely low due to an imperfect focal length, and the channel SNR is unstable due to rapid channel variations as a result of mobility. Unlike RF systems, the decrease in SNR of each optical communication link during movement was resolvable until now. While RF users can freely move around without significantly reducing the signal strength, any optical lens misalignment can cause a sharp drop of SNR and an immediate LiFi connection loss.
- The third challenge is to identify TXs when their signals are mixed. Particularly, when the links between the TX, RX, and lens are imperfectly aligned (this always happens in a mobile context). Several light beams coming from different TXs may interfere each other, and the signals from different TXs may be mixed together. Typical modulation schemes cannot support demodulation when the signals are randomly mixed. This partly explains why LC is sensitive to the optical frontend alignment condition in the mobile scenario, especially when multipoint-to-point (M2P) support is required. Accordingly, it raises a requirement of new modulation waveforms so that the RX can identify TXs even if the signals are optically mixed.

It is also challenging to maintain seamless M2P connectivity and the communication quality while the devices are freely moving. This requires receiver to track and trace the interested transmitters for adapting its system for any random movement.

This paper aims to solve the above mentioned challenges, including the light source sensing and mobility support abil-

ities. By introducing a novel LiFi system that consists of a novel hybrid waveform, a novel RX architecture along with sensing platforms for mobility adaption, there are numerous benefits of the system include:

- Within a novel hybrid waveform concept, the identification (ID)-signaling stream helps RX to detect TXs among other noisy sources. There is no need to send pilot frames [5], thus it reduces the signaling overhead. The ID-signaling stream uses frequency shift keying (FSK) modulation. In addition, the RX is equipped with a novel 'TXs sensing platform' that provides a high performance of detecting and identifying TXs when the channel SNR is extremely low (e.g., the channel SNR is less than -10 dB). Importantly, the novel hybrid waveform concept allows RX identifying TXs even if their signals are optically mixed.
- A novel RX architecture is proposed by using a digital mirror device (DMD). The DMD (together with a controllable lens located in front of the DMD) offers the RX the ability to scan and detect the positions of light sources in three-dimension space and provides the flexible M2P configuration. The RX is equipped with a novel 'mobility sensing platform' so that the RX can track the movement of TXs and maintain communication links.
- Additionally, the hybrid waveform concept uses a augmented spectral efficiency discrete multitone (ASE-DMT) modulation scheme for modulating its high-rate data stream at a high spectral efficiency [4]. The overall spectral efficiency of the hybrid waveform is higher than that of ASE-DMT due to the additional contribution of the ID-signaling stream [13]. Moreover, dimming abilities without reducing the SNR is also an interesting feature of the proposed waveform (dimming is also necessary for infrared LiFi as it reduces the optical power).

There are numerous related works in the field. Related to dual-mode waveforms, a notable one is the "twinkle variable pulse position modulation (VPPM)", termed "twinkle VPPM", within the IEEE 802.15.7-2018 standard, which allows for a high speed optical camera communications (OCC) with region-of-interest image processing capability [6]. A dual-mode waveform by Nguyen *et al.*, [7] is designed for a hybrid receiver consisting of a camera and a PD. Overall, the existing dual-mode waveform methods use a rectangular shaped waveform because of its simplicity. This work introduces a dual-mode LiFi waveform (hybrid waveform), which composes of a high-rate LiFi stream that uses a superimposed modulation for a spectral efficiency and a low-rate LiFi stream that uses FSK modulation for the sensing capability.

In terms of mobility support, currently, various acquisition, tracking, and pointing (ATP) mechanisms for LC to deal with mobility also exist. A comprehensive survey in [8] highlights several ATP methods for LC, including (i) controllable mirror, (ii) gimbal, (iii) beam splitter, mirrors and a tracking sensor, (iv) adaptive optics, (v) liquid crystal, and (vi) combined RF-optical wireless communications (OWC) tracking solution. Among these, the mirror solution offers a wide field-of-view (FoV) for tracking the communication sources. Unlike the existing works that use the DMD as a reflecting surface to steer the light beam's direction [9], this work uses the DMD as a crucial part of RX to support the M2P protocol and mobility. As being integrated into the receiver, it has the full ability to control millions of micro-mirrors within the DMD according to the channel condition. This advantage has been taken specifically in the proposed sensing platforms within the RX: a 'TXs sensing platform', which aims to sense transmitters, and a 'mobility sensing platform', which aims to support multiple mobile users. A 'TXs sensing platform' offers the RX the ability to detect data-transmitting light sources among noisy sources, and identify light sources from different networks. A 'mobility sensing platform' offers the RX the ability to detect movement and trace light sources, maintaining the seamless connectivity of simultaneous links while moving. The remainder of this paper is organized as follows. Section II explains the system architecture and the operation of proposed algorithms. Section III provides the simulation results. Finally, section VI concludes this work.

II. System Description

A. Waveform Design

The proposed hybrid waveform is a combination of a high-speed multicarrier stream and a low-speed rectangular shaped signal stream. A superposition modulation scheme called ASE-DMT [4] is used for the high speed data stream, while a FSK is used for the low rate data stream. The hybrid waveform is expressed as follows:

$$y(t) = x(t)\, s(t/N) \tag{1}$$

where $x(t)$ is the unipolar signal (particularly, the superimposed ASE-DMT signal is used in the proposed system for a high spectral efficiency), $s(t/N)$ is the rectangular shaped FSK signal, and $N > 1$ is the ratio between the modulation clock rates of the ASE-DMT and the FSK signals.

In (1), the low rate signal $s(t/N)$ modulates the ID of the light source, thus it is called the ID-signaling stream. It plays a role as the pulse-width modulation (PWM) dimming wave when being applied to the unipolar ASE-DMT signal $x(t)$ with a length of N samples. For example, when $s(t/N) = -1$, it reverses the unipolar signal $x(t)$ and produces a bright frame. Conversely when $s(t/N) = 1$, it produces a dimmed frame. Note that the waveform integration is not applicable to bipolar signals (such as direct-current biased optical orthogonal frequency division multiplexing (DCO-OFDM)) because the ID signal $s(t/N)$ is not decodable in such a case. Therefore, the waveform integration can also be referred to as the modulation of the PWM dimming wave. This method will not reduce any LiFi communication link budget (including both the data rate and the SNR performance) due to the PWM dimming property.

Fig. 1 shows examples of the hybrid waveform in two cases that demonstrate how to integrate the FSK signals to the ASE-DMT waveform. The top sub-figure uses a FSK signal

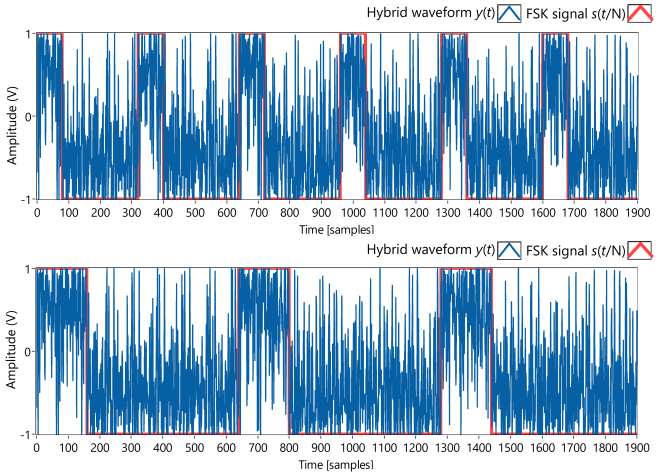

Fig. 1. Two examples of hybrid waveform. The FSK frequency equals 1/4 (top) and 1/8 (bottom) of the ASE-DMT frame rate. Both cases use the PWM dimming at 25%.

that its interval equals to $4\times$ the length of an ASE-DMT frame. Similarly, the bottom sub-figure use FSK signals that its interval are $8\times$ the ASE-DMT frame length. These waveforms can be used to identify two different light sources. In the cases that the number of TXs is greater than the number of FSK frequencies available, one ID can be mapped by a sequence of multiple FSK frequencies.

B. System Architecture

The proposed RX architecture is designed to receive data from multiple TXs simultaneously. The key functions of the RX, including sensing platforms and controlling blocks, are shown in Fig. 2. The RX composes of a front-lens, a DMD, and PDs with lenses (back-lenses). A front lens aims to spatially separate the incoming beams from different light sources. This front lens is a non-imaging lens because it produces a certain size for each light spot displayed on the DMD so that RX can track the light spots' movement. Next, a DMD consisting of millions of micro-mirrors can adjust their orientations to direct the beams onto different PDs. The area of the DMD that contains the micro-mirrors with their orientations being controlled is referred to as the 'activate area', while the remaining area of the DMD is inactivated. Notice that, within RX, there are multiple PDs that are used to receive data coming from different transmitters (PD-1 and PD-2 in Fig. 2) and a specific PD that is used for sensing only, namely a "sensing-PD". This sensing-PD will observe the light energy coming from the entire inactive area of the DMD. When a light spot is moving out of the DMD active area, the sensing-PD can detect the movement from the increase of energy. Lastly, each light beam is concentrated by a back-lens to focus the optical energy onto a PD (or a set of PDs for each light beam, depending on the multiple-input-multiple-output configuration). This back lens is an imaging lens and it targets a maximum achievable SNR for communications.

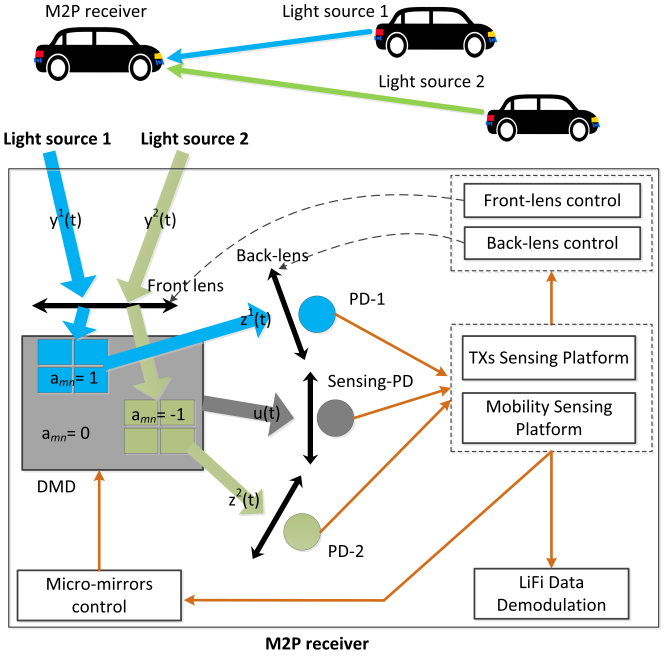

Fig. 2. A schematic architecture of the proposed RX. On the DMD, two active areas of micro-mirrors (blue and green clusters) control the orientation of micro-mirrors to reflect light beams onto two data PDs, while the remaining inactive area (gray area) reflects the light onto the sensing-PD.

The configuration of the orientations of micro-mirrors is executed via the activation function a_{mn}, where integers $m \subset [1, M_0]$ and $n \subset [1, N_0]$ are the horizontal and vertical indexes of the micro-mirrors, and $M_0 \times N_0$ is the DMD resolution. Particularly, $a_{mn} = \pm 1$ when the micro-mirror indexed mn is activated. Otherwise, $a_{mn} = 0$ when the micro-mirror indexed mn is inactivated. Accordingly, for the configuration of two simultaneous links, two data-PDs, PD-1 and PD-2, can use two activated orientation options with $a_{mn} = \pm 1$ (ON and OFF states of micro-mirrors), while the sensing-PD uses the inactivated orientation option with $a_{mn} = 0$ (the zero-shifted degree).

All micro-mirrors within an activate DMD area will follow the same orientation (corresponding to $a_{mn} = 1$ or $a_{mn} = -1$) to collect the light signal. The sum of light signal from the light spot indexed d being collected by a data-PD indexed d is expressed as $z^d(t)$. Due to mobility and noise, the position of an DMD area being activated to collect the signal may not be the same as the position of the light spot; thus the received signal $z^d(t)$ is not always equal to the transmitted signal $y^d(t)$. The parts of signals that are leaking out of the active DMD areas will be collected by the sensing-PD and be expressed as follows:

$$u(t) = \sum_{d=1}^{2} \sum_{m=1}^{M_0} \sum_{n=1}^{N_0} \{1 - |a_{mn}^d|\}\, y_{mn}^d(t) = \sum_{d=1}^{2} \{y^d(t) - z^d(t)\} \tag{2}$$

where a_{mn}^d is the activation function of a micro-mirror indexed

mn within the active DMD area indexed d ($1 \leq d \leq 2$).

C. Operation of "TXs sensing platform"

The procedure of *TX sensing platform* can be summarized in **Algorithm 1**, where $\mathcal{S}$ is the set of DMD areas that finds individual light spots; $\mathcal{F}$ is the set of FSK symbols that are found in the DMD subareas $\mathcal{S}$. In addition, $\mathcal{K}$ is the intermediate set of DMD subareas to search for signal; k is a specific subarea (a cell) that is searching for signal. The waveform $u(t)$ will be used for sensing the appearance of transmitters, while the signals received from data-PDs can be ignored.

To search for the FSK signals from the received waveform $u(t)$, Gabor transform, which is a special case of short-time Fourier transform [10], is used to observe the signal in the frequency-time domain. The interested frequencies can be extracted efficiently while the noise (including the white noise, direct-current noise, and other out-of-interest frequencies) can be eliminated. Gabor coefficients apply a simple pre-processing technique as a better way to identify FSK signals, which includes a hard threshold and an average process.

The DMD starts with a low resolution (1×1) to search the appearance of FSK signals. If the receiver finds a mix of FSK signals within a specific DMD subarea (which means that the light spots are not separated within this subarea), it loops to increase the resolution of that subarea (by a factor of 2 for each horizontal and vertical dimensions) until the light spots are spatially separated, while ignoring the remaining subareas that do not find any interested FSK signal. This is an adaptive-resolution searching mechanism that can boost the speed for detecting and identifying TXs.

D. Operation of 'Mobility sensing platform'

After the transmitters are detected and their light spots on the DMD are spatially separated, the data-PDs will collect the light signals for demodulation while the mobility sensing procedure can be executed. The receivers observes the energy entropy $\triangle$E, which is equal to the energy change of the $u(t)$ signal caused by mobility. The mobility sensing procedure includes three steps. Firstly, by observing the energy entropy $\triangle$E, mobility is detected. After that, an omnidirectional extension process will extend the DMD activate areas to detect the movement diameter D. Finally, an unidirectional scanning process (a blind scanning by shifting an activate DMD area by a diameter D from the last position to a specific angular direction a) will trace the movement direction of the light sources, and then update the DMD activate areas to the latest positions of light spots (one activate area corresponds to one light spot). Due to the limited space, details of this platform are not included in this paper.

III. Computer Simulations

A. Results of TX sensing platform

An example of a FSK signal in an extremely noisy channel condition (channel SNR of -12 dB) is shown in Fig. 3. When applying Gabor transform and a simple processing technique

Algorithm 1: TX Sensing Algorithm

Initialize: initial $\mathcal{K}$ has one element k, initial k equals the entire DMD area, $loop$ =TRUE
$\mathcal{S} = \mathcal{F} = \emptyset$
Activate the sensing-PD to receive signal
While ($loop$ =TRUE): ▷ {Re-scan at a higher resolution if there are mixed signals}
For ($k \subset \mathcal{K}$): ▷ {Observe the DMD cell k}
  Divide the cell k by 4 into smaller cells $[k_1, k_2, k_3, k_4]$
  For ($1 \leq i \leq 4$):
    Control micro-mirrors within the cell k_i
    Collect the signal $u_i(t)$ that is reflected from the cell k_i
    Gabor transform the signal $u_i(t)$
    Apply threshold and average the Gabor coefficients
    Search for FSK signals, r_x is the resulting symbol
    Switch (r_x):
      Case 1: ($r_x \neq$ Null) ▷ {there is FSK signal}
        If (There is a mix of FSK symbols)
          Add k_i to set $\mathcal{K}$
          $loop_i$ =TRUE
        Else ▷ {unique FSK symbol $r_x = f_i$}
          Add k_i to set $\mathcal{S}$
          Add f_i to set $\mathcal{F}$
          $loop_i$ =FALSE
      Case 2: (r_x = Null) ▷ {there is no signal}
        $loop_i$ = FALSE
  End For
  $loop_k = \text{OR}\{loop_i\}, i \subset [1, 4]$
End For
$loop = \text{OR}\{loop_k\}, k \subset \mathcal{K}$
Output: $\mathcal{S}$, $\mathcal{F}$

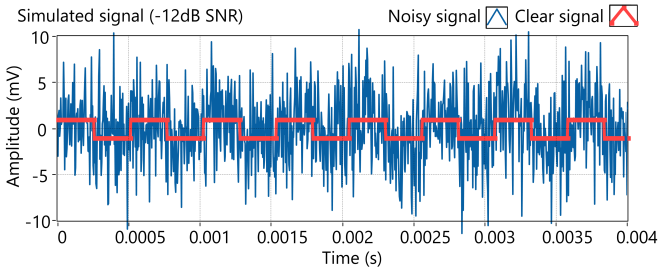

Fig. 3. Example of an FSK signal with a simulated channel SNR of -12 dB.

(a hard threshold), most of the background noise can be removed and the FSK signal can be detected as shown in Fig. 4. The average spectrum over the observed time can be obtained as shown in Fig. 5. It displays more clearly the peak-energy frequency from the noise floor, and the FSK signal is detected at a better bit error ratio (BER) performance. The FSK sensing performance is evaluated in a simulation, in which each light source uses one FSK symbol for its ID

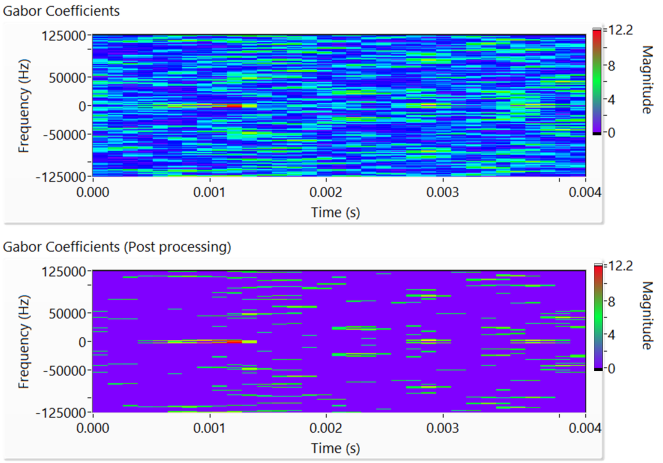

Fig. 4. Example of Gabor coefficients transformed from the FSK signal in Fig. 3 before and after processing (channel SNR of -12 dB is used).

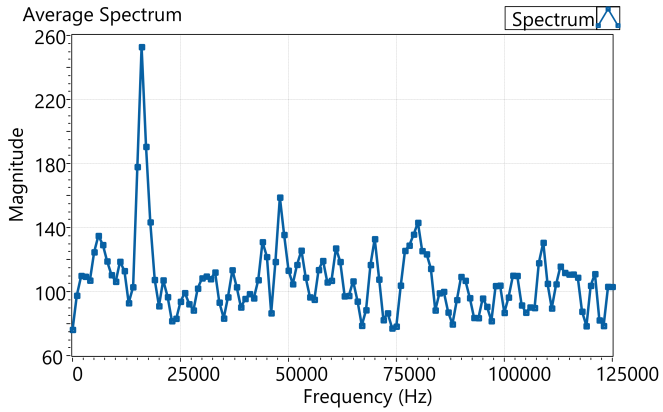

Fig. 5. Example of average spectrum from the processed Gabor coefficients in Fig. 4. The observed duration is $1/240$ s, channel SNR of -12 dB is used, and the transmit FSK frequency between the FSK signaling band 0 kHz to 125 kHz is detected.

signaling. There are cases that cause error as listed in (3).

$$\text{Error:} \begin{cases} t_x \neq f_i, r_x = f_i, & \begin{cases} t_x = f_{j\neq i}, r_x = f_i \\ t_x = \text{Null}, r_x = f_i \end{cases} \\ t_x = f_i, r_x \neq f_i, & \begin{cases} t_x = f_i, r_x = f_{j\neq i}, \\ t_x = f_i, r_x = \text{Null}, \end{cases} \end{cases} \tag{3}$$

where t_x is the transmitted symbol; r_x is the received symbol; f_i and $f_{j\neq i}$ are two different FSK signals; 'Null' denotes that there is no signal. The error probability cases $p\left(t_x = f_i, r_x = f_{j\neq i}\right) = p\left(t_x = f_{j\neq i}, r_x = f_i\right)$ show that the identification of the FSK symbol is wrong under an assumption that there is a signal. Let's denote p_1 as the error probability for these two cases. The remaining two cases in (3) represent the error cases that RX incorrectly detects 'there is FSK signal' ($r_x \neq$ Null). Overall, all four cases in (3) produce an accumulate error probability which is denoted as p_2.

When a commercial DMD with a refresh rate of 240 Hz [11] is used, the time interval of 1/240 second is used to

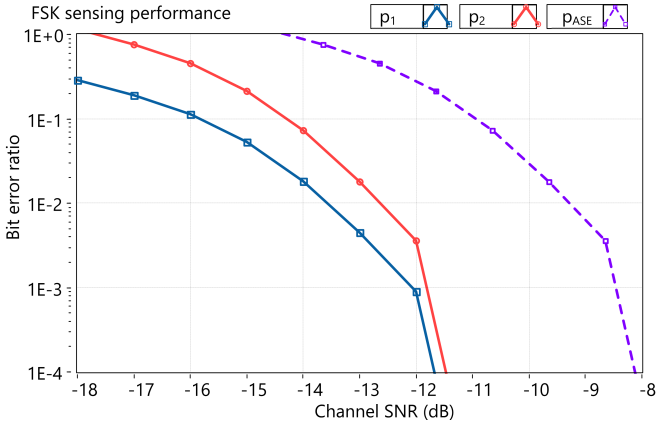

Fig. 6. Simulated FSK sensing performance: error ratio of wrong FSK identification (blue line) and accumulate error ratio of FSK detection and identification (red line), FSK-sinaling with ASE-DMT (dash purple line). The duration of $1/240$ s is used to observe the signal.

observe the signal and detect the transmitter. Due to the restricted relationship between the clock rates of the FSK signal and the hybrid signal as given in (1), when considering a 20 MHz communication bandwidth and the ASE-DMT frame size is 80 samples length, the observed duration allows for $(1/240)/(2 \times 80/20M) = 520$ FSK frequencies to be used. For a simple evaluation of the sensing error, several FSK frequencies are chosen, including $\{f_0, f_0/2, f_0/4, f_0/8, f_0/16, f_0/32, f_0/64\}$, where f_0 equals to 125 kHz, which is half the clock rate of the PWM dimming wave used in the 20 MHz clocking hybrid signal. With these parameters, the simulation results of p_1 and p_2 of the proposed TX sensing platform are shown in Fig. 6. Results show that an error ratio of below 10^{-4} is achieved in an extremely low channel SNR condition of -11 dB, for all results, showing the reliable light sources identification performance based on the proposed algorithm. Note that, when applying FSK to the signaling waveform in addition to the ASE-DMT, the peak-to-peak amplitude of FSK reduces to 0.68 times that of the FSK alone due to the characteristic of the ASE-DMT waveform. This causes an SNR reduction of 3.35 dB.

The simulation results in Fig. 6 do not include the case of a mix of two-or-more FSK carriers. However, by observing the signal in the frequency-time domain, the case with mixed-signals does not reduce the performance of identifying whether there is FSK signal or not because the energy of the interested frequency is maintained. After detecting the mixed signals, the RX can adjust its optical front-end to ensure the spatial separation of light spots on the DMD.

B. Results of Mobility sensing platform

In the simulation of the *mobility sensing platform*, there are two light spots (already separated on the DMD) at different sizes (the size displayed on the DMD) being used, and their movements are random. The maximum resolution of DMD of 100×100 is used to trace the movement of TXs. The channel SNR of 20 dB is used to simulate the channel SNR condition

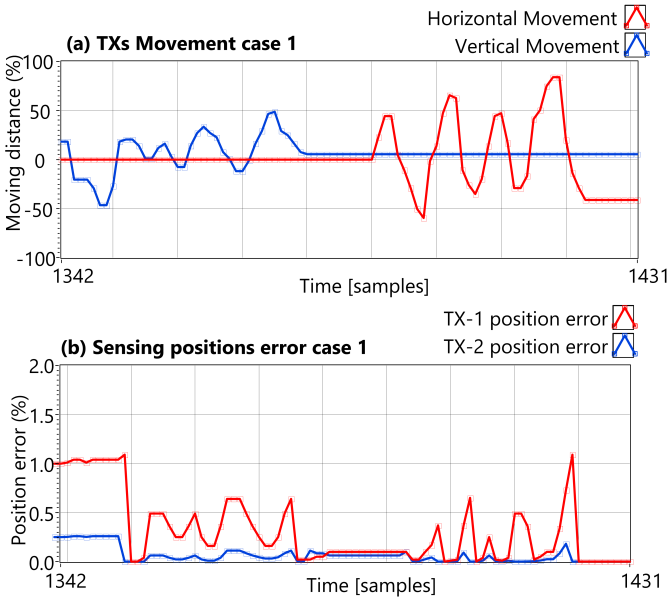

Fig. 7. The performance of mobility sensing platform when the DMD energy loss ratio (caused by the optical link instability) is randomly generated within 10%.

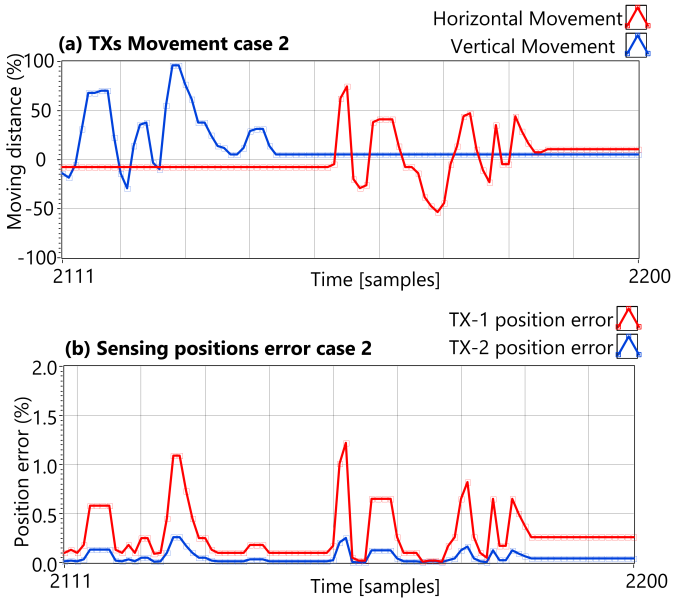

Fig. 8. The performance of mobility sensing platform when the DMD energy loss ratio (caused by the optical link instability) is randomly generated within 20%.

based on practical measurements in [12]. The unstable optical alignment condition is simulated by applying random energy loss cases of 20% or less to the signal. The results in Figs. 7 and 8 show that, despite the cases of random movement of light spots and the unstable optical alignment conditions, the error performance of tracing the TXs positions is still guaranteed. It is less than 2% compared to the diameter of light spots on the DMD, for all considered cases. When we assume that the energy of light is equally distributed over the area of the light spot on the DMD for simplicity, this results in an additional loss of less than 4% of the signal energy errors in detecting the position of the light spot.

Finally, simulation results of transmitters detection and mobility support are provided; however, it needs further practical validation for multi-user support in real-world scenarios.

IV. Conclusions

This work proposes a novel system architecture for mobile M2P LiFi connectivity. Relying on a novel hybrid LiFi waveform, the details of a novel RX architecture using DMD to support simultaneous links and two sensing platforms to support mobility are provided. Simulation results have proved that the sensing techniques can support mobile and seamless M2P links. Particularly, the TXs sensing platform shows an error rate of below 10^{-4} achieved in an extremely low channel SNR condition of -11 dB. The mobility sensing platform also shows a reliable performance. The signal energy loss due to the movement is below 4% for all movement cases.

From the simulation results, the practical implementation of mobile M2P links link will be the subject of future work.

References

[1] H.Haas, E. Sarbazi, H. Marshoud, J. Fakidis, "Chapter 11 - Visible-light communications and light fidelity," in *Optical Fiber Telecommunications VII*, Academic Press, 2020, p. 443-493, ISBN 9780128165027.

[2] H. Haas, J. Elmirghani, and I. White, "Optical wireless communication," in *Philosophical Transactions of the Royal Society A: Mathematical, Physical and Engineering Sciences*, vol. 378, pp. 20200051, 2020.

[3] Dana Hull, "Tesla phases out radar sensors, shifts to camera-based Autopilot, [Online]", May 26, 2021, www.ttnews.com/articles/tesla-phases-out-radar-sensors-shifts-camera-based-autopilot

[4] M.S. Islim, H. Haas, "Augmenting the spectral efficiency of enhanced PAM-DMT-based optical wireless communications," in *Opt Express*, 2016 May 30, 24(11):11932-49.

[5] Hamid Hemmati, and David Caplan, "Chapter 4 - Optical Satellite Communications," in *Optical Fiber Telecommunications Volume VIB*, 6th Edition, Academic Press, May 2013, p. 121 -162, ISBN 9780123972378.

[6] R. D. Roberts (Intel Corp.), "IEEE 802.15.7r1 - Intel OCC Proposal," in *IEEE Standards Association*, Jan. 2016, [Online], https://bit.ly/3dUL7ZK

[7] D. T. Nguyen, S. Park, Y. Chae, and Y. Park, "VLC/OCC Hybrid Optical Wireless Systems for Versatile Indoor Applications," in *IEEE Access*, vol. 7, pp. 22371-22376, 2019.

[8] Y. Kaymak, R. Rojas-Cessa, J. Feng, N. Ansari, M. Zhou and T. Zhang, "A Survey on Acquisition, Tracking, and Pointing Mechanisms for Mobile Free-Space Optical Communications," in *IEEE Communications Surveys & Tutorials*, vol. 20, no. 2, pp. 1104-1123, Secondquarter 2018.

[9] A. M. Abdelhady, A. K. S. Salem, O. Amin, B. Shihada and M. -S. Alouini, "Visible Light Communications via Intelligent Reflecting Surfaces: Metasurfaces vs Mirror Arrays," in *IEEE Open Journal of the Communications Society*, vol. 2, pp. 1-20, 2021.

[10] Wikipedia, *Gabor transform*, [Online]. Available: https://en.wikipedia.org/wiki/Gabor_transform

[11] Texas Instruments, *DLP product - getting started*, [Online]. Available: https://www.ti.com/dlp-chip/getting-started.html

[12] T. Nguyen, M. S. Islim and H. Haas, "Integration of Dimming into LiFi Systems," in *2020 IEEE 91st Vehicular Technology Conference (VTC2020-Spring)*, Antwerp, Belgium, 2020, pp. 1-5.

[13] T. Nguyen, M. S. Islim, and H. Haas, "A hybrid OCC-LiFi system with dimming capability", in *2021 IEEE 94th Vehicular Technology Conference (VTC2021-Fall)*, 2021.